

Exploring the Binding of Inhibitors Derived from Tetrabromobenzimidazole to the CK2 Protein Using a QM/MM-PB/SA Approach

Marius Retegan,* Anne Milet, and Hélène Jamet*

Département Chimie Moléculaire, UMR-5250, ICMG FR-2607, CNRS Université Joseph Fourier BP 53, Grenoble, France

Received December 8, 2008

We present an adaptation of the MM-PB/SA method for the estimation of binding free energies in protein–ligand complexes simulated with QM/MM molecular dynamics. The method is applied to understand the binding of a set of tetrabromobenzimidazole inhibitors to the CK2 protein. We find that the QM/MM interaction energy alone cannot always be used as a predictor of the binding affinity, and the inclusion of solvation effects via the PB/SA method is essential in getting reliable results. In agreement with experimental observations, we show that the van der Waals interactions are the driving force for the binding, while the electrostatic interactions orient these inhibitors in the CK2 active site. Additionally a per-residue energy decomposition analysis was applied to determine the individual contributions to the protein–inhibitor interaction. Based on these results, we hypothesize that the inclusion of a sufficiently large polar group on the tetrabromobenzimidazole skeleton could increase the binding affinity. The results show that the QM/MM-PB/SA method can be successfully employed to understand complicated structure–activity relationships and to design new inhibitors.

INTRODUCTION

Understanding the subtle interactions that govern protein–inhibitor binding is an important goal in rational drug design. In the last decades, steady progress was made in developing methods for a rapid and accurate determination of properties that include structural features and binding interaction energies.¹ Although empirical scoring functions based on two- or three-dimensional quantitative structure–activity relationship (QSAR) are very useful for high-throughput virtual screening, they often neglect conformational flexibility of the protein, desolvation, and entropic effects associated with the binding process.² Beyond the methods based on scoring functions we find techniques that use molecular dynamics (MD) or Monte Carlo (MC) simulations to sample the conformational space of the protein–inhibitor system. Free energy perturbation (FEP) and thermodynamic integration (TI) are the most rigorous and accurate methods to compute free-energy changes,^{3,4} but they are computationally expensive. Therefore, more approximate methods have been developed, e.g. the linear interaction energy (LIE)^{5,6} method and the molecular mechanics Poisson–Boltzmann/surface area (MM-PB/SA) method.⁷ Although computationally efficient for large systems, the molecular mechanics (MM) potential energy function combined with empirically derived parameters, that are commonly used in these methods, have several drawbacks. One limitation of standard nonpolarizable force fields is the neglect of electronic polarization of the protein environment exerted on the inhibitor and vice versa. These charge effects can be important in order to understand the protein–inhibitor interactions.^{8–10} Another limitation is

that each new inhibitor must be parametrized and tested, which can be time-consuming.

In the last three decades, combined quantum mechanics and molecular mechanics (QM/MM) methods have been used to elucidate numerous problems in the simulation of biological systems.^{11–15} Only recently hybrid methods have started to emerge as an alternative route for the computation of properties in rational drug design.¹⁶ These approaches combine a QM model for the inhibitor which avoids the development of specific parameters, while the protein and the solvent are represented by a MM force field which is computationally efficient. With a QM definition of the inhibitor, polarization effects are taken into account by adding an electrostatic term to the Hamiltonian that represents the protein and solvent by a set of point charges. A number of recent studies have used QM/MM methods to investigate the specific nature of protein–inhibitor interaction in matrix metalloprotease (MMP-9),¹⁷ HIV-1 protease,⁹ CDK2,¹⁸ and HIV-1 integrase.¹⁰

A few years ago, Gräter et al. were the first to use QM/MM combined with PB/SA for the study of binding free energy of trypsin complexed with benzimidinium derivatives and FKBP inhibitors.¹⁹ The ensemble used by the authors for the evaluation of the binding free energy was obtained via a docking protocol in the case of benzimidinium derived inhibitors while for the FKBP inhibitors was obtained including experimental data. The accuracy of the prediction was higher if the FKBP inhibitors were included in the data set (correlation coefficient = 0.56), compared to only the benzimidinium derived inhibitors (correlation coefficient = 0.20). The authors concluded that the predicted binding affinities are influenced by the quality of the structures used. In the present paper, we used a similar QM/MM-PB/SA method to calculate protein–inhibitor binding free energies,

* Corresponding author e-mail: marius.retegan@ujf-grenoble.fr (M.R.), helene.jamet@ujf-grenoble.fr (H.J.).

with the difference that the conformational ensemble was obtained from a QM/MM MD simulations. Although not related to drug design, a very recent article by Kaukonen et al.²⁰ showed that a QM/MM-PB/SA method reproduces the results of a strict QM/MM FEP method for the evaluation of free energies of reactions in proteins.

This method was applied to the CK2 protein complexed by different inhibitors derived from tetrabromobenzimidazole. CK2 is an acronym derived from the misnomer “casein kinase 2”. More than 500 different protein kinases are encoded in the human genome.²¹ The similarity of the reaction mechanism has proven to be a major obstacle in developing specific inhibitors. CK2, which catalyzes the transfer of the γ phosphate of ATP to serine and threonine residues of protein substrates, is the most pleitropic protein kinase known to date. It has more than 300 substrates already identified, many of which are involved in signal transduction, gene expression, and DNA synthesis and repair.²² The elevated activity of CK2 in a number of tumors,²³ in conjunction with the observation that many viruses rely on it to perform phosphorylation of the proteins essential to their life cycle, makes CK2 a potential target for antineoplastic and antiinfectious drugs.

Consequently a number of ATP site directed inhibitors in the low micromolar range were described in the literature. Among these inhibitors, TBB (4,5,6,7-tetrabromobenzotriazole) has proven to be one of the most successful for in cell and *in vivo* studies.²⁴ Recently the efficiency of TBB was improved by replacing the triazole ring by an imidazole, functionalized with a variety of polar functions.²⁵ The crystal structures of CK2 with different inhibitors and mutational analysis show a series of bulky residues which make the ATP binding site smaller in CK2, compared to other protein kinases.^{26–29} It is likely that the remarkable selectivity of TBB toward CK2 among a panel of more than 30 protein kinases³⁰ is attributed to this fact.

We applied the QM/MM-PB/SA method for the estimation of binding free energy to gain further insight into the specific binding interactions between CK2 and a number of inhibitors derived from tetrabromobenzimidazole/benzotriazole. The specific protein–ligand interactions were identified by a subsequent decomposition of the van der Waals and electrostatic interaction energies in terms pertaining to each amino acid. The results obtained for these systems are in good agreement with experimental data and suggest that the QM/MM-PB/SA method is a viable approach for dissecting complicated protein–ligand interactions.

METHODS

Construction of the Initial Models of the CK2-Inhibitor Complexes. We have studied 5 inhibitors, all of which share a common core structure (Table 1). The inhibitors are named in conjunction to their relative inhibition power toward CK2, with L1 being the most potent one and L5 the least potent inhibitor. Their experimental inhibition constants are all taken from the same reference.²⁵ The structure of CK2 complexed with 4,5,6,7-tetrabromo-N,N-dimethyl-1H-benzimidazol-2-amine (L1) (PDB code: 1ZOE)²⁸ was used as a template to construct the initial models for the other complexes. This was accomplished with the MOLDEN package.³¹ It should be noted that the crystal structure of

Table 1. Inhibitor Activity against the CK2 for the Inhibitors Studied in This Work

Id.	Structure	$K_i(\mu\text{M})$
L1		0.04
L2		0.07
L3		0.23
L4		0.40
L5		1.90

CK2 complexed with L2 (PDB code: 1ZOG)²⁸ and L4 (PDB code: 1J91)²⁷ were also available. The former structure was chosen because of its higher X-ray resolution: 1.77 Å compared with 2.30 and 2.22 Å for CK2-L2 and CK2-L4, respectively. For the protein, the hydrogen atoms were placed according to the predicted pK_a of the amino acids at a pH of 7 using PDB2PQR,³² which assigns protonation states based on pK_a values calculated with PROPKA 2.0.³³ In the case of histidine residues this gave protonation of the $N^{δ1}$ atom for residues 105, 236, 309, and 321 and protonation of the $N^{ε1}$ atom for residues 148, 154, 160, 166, 183, 239, 276, and 291. The rest of the acidic and basic residues were assumed to be charged. The total charge of the protein is +1.

Hybrid Potential Simulations. All simulations were performed using the fDynamo library.³⁴ The semiempirical AM1 model³⁵ was used to describe the inhibitors, while the OPLS-AA force field³⁶ was adopted for the protein and the three-point TIP3P model³⁷ for water. The semiempirical description can be quite inaccurate in some cases, and it will be ideal to use a higher level ab initio method to describe the inhibitor. However, these calculations are still too time-consuming to be practical for drug design studies. A careful analysis is necessary to validate a semiempirical QM/MM model, and in our case this done by comparing our simulation results with the crystal structures, when they were available. The protein was placed in a cubic box with a margin of 10 Å along each dimension. An appropriate number of counterions were added to neutralize the system. The entire system was then minimized by performing 1000 steps of CG (conjugate-gradient). Afterward, the system was equilibrated for 1 ns by using Langevin-Verlet MD simulations (NVT ensemble) at 300 K. The time step for the simulations was

1 fs. A friction coefficient of 2 ps^{-1} was employed for all atoms. The electrostatic and Lennard-Jones interactions were calculated using an atom-based force-switching method with inner and outer cutoff of 8 and 12 Å, respectively. The Lennard-Jones parameters for the QM atoms were taken from the OPLS-AA force field, which in the case of bromine atoms have a value of 3.47 Å for σ and 0.47 kcal/mol for the depth of the potential well, ε . In the MD simulation, amino acid residues more than 18 Å away from the inhibitor were fixed. A subsequent 0.5 ns production run was performed using the same setup, giving a total simulation time of 1.5 ns. Using the presented setup, the production run for CK2 complexed with L1 took approximately 5 days on an Intel (R) Xeon (TM) at 2.60 GHz processor.

QM/MM-PB/SA Calculations. Experimentally, the potency of an inhibitor is measured in terms of the inhibition constant K_i . This value can be related to the change in free energy of binding with the equation $\Delta G = k_B T \ln K_i$, where k_B is the Boltzmann constant, and T is the absolute temperature.

The MM-PB/SA method has successfully been applied for the estimation of binding free energies of drug candidates to proteins.⁷ In the classical approach developed by Kollman et al., separated snapshots of the inhibitor, the protein, and the protein–inhibitor complex are taken from a MD trajectory of the complex. The counterions and water molecules are removed, and the free energy is computed separately for each snapshot using the following equation:

$$G = G_{\text{gas}} + G_{\text{solv}} = (E_{\text{int}} + E_{\text{elec}} + E_{\text{vdW}} - TS) + (G_{\text{PB}} + G_{\text{SA}}) \quad (1)$$

where E_{int} is the internal energy arising from bonds, angles, and torsion angles terms; E_{elec} is the electrostatic energy; E_{vdW} is the van der Waals energy; G_{PB} is the polar solvation free energy, calculated with a numerical solution of the Poisson–Boltzmann equation; G_{SA} is the nonpolar solvation energy, estimated with a simple surface area term; T is the temperature; and S is the gas-phase entropy contribution which can be estimated with the normal-mode analysis or quasi-harmonical analysis.

In this single trajectory approach, E_{int} cancels out, and an estimation of the binding free energy can be obtained by using the following equation:

$$\Delta G = G_{\text{complex}} - (G_{\text{protein}} + G_{\text{inhibitor}}) = \Delta E_{\text{elec}} + \Delta E_{\text{vdW}} + \Delta G_{\text{PB}} + \Delta G_{\text{SA}} - T\Delta S \quad (2)$$

If one is interested in estimating relative binding energies for a series of compounds with similar structures, the entropic term ($-T\Delta S$) can be omitted.³⁸ Within this approximation the relative binding energy for two inhibitors is:

$$\Delta\Delta G = \Delta G_1 - \Delta G_2 = \Delta\Delta E_{\text{elec}} + \Delta\Delta E_{\text{vdW}} + \Delta\Delta G_{\text{PB}} + \Delta\Delta G_{\text{SA}} \quad (3)$$

Our approach differs from the one developed by Kollman et al. since the system is represented by a hybrid potential. This means that the electrostatic term from eq 2 is computed at a quantum mechanical level:

$$\Delta E_{\text{elec}} = \langle \Psi | \mathcal{H}^{\text{QM/MM}} | \Psi \rangle + \langle \Psi | \mathcal{H}^{\text{QM}} | \Psi \rangle - \langle \Psi_0 | \mathcal{H}^{\text{QM}} | \Psi_0 \rangle \quad (4)$$

where Ψ represents the polarized wave function of the inhibitor due to the presence of the protein environment, Ψ_0 is the wave function of the inhibitor in the gas phase, $\mathcal{H}^{\text{QM/MM}}$ is the Hamiltonian used for describing the electrostatic interaction between the QM and MM parts, and \mathcal{H}^{QM} is the gas-phase Hamiltonian for the selected QM method.

For each protein–inhibitor complex, a total of 51 equispaced snapshots were taken from the last 0.5 ns of the MD trajectory. The fDynamo library was used for the computation of the nonbonded interactions for which an infinite cutoff was employed.

The electrostatic contribution to solvation was estimated using the DELPHI software.³⁹ Grids dimensions $169 \times 169 \times 169$ were used. The coarse density maps calculated with a scale of 0.5 grids/Å and Coulomb boundary conditions were subsequently refined in by reducing the spacing to 2 grids/Å. Charges and van der Waals radii were taken from the OPLS-AA force field. Because the force field defines σ , but not van der Waals radii per se, the atomic radii were taken to be half of the values of the Lennard-Jones σ parameter, except for the hydrogens where we used a value of 1.15 Å. In the case of the inhibitor, the charges were derived by ab initio electrostatic surface potential (ESP) calculation (HF/6-31G*), using the CHELPG module from the Gaussian 03⁴⁰ software package. The dielectric constant was set to unity for the solute and 80 in the case of the solvent.

The nonpolar contribution to solvation was estimated using fDynamo with a solvent probe radius of 1.4 Å. This term was then used to compute the solvent-accessible surface area (SASA) with the equation $G_{\text{SA}} = \gamma \times \text{SASA} + \beta$,⁴¹ where γ and β are empirical constants, and in this work they were set to 0.0054 and 0.92 kcal/mol, respectively.

For evaluation of different terms, scripts have been developed, making the process easily applicable to other systems.

Residue-wise Interaction Energy Decomposition. An amino acid decomposition analysis was carried out in order to investigate the specific interactions that the CK2 protein establishes with this family of inhibitors. The van der Waals and electrostatic energy were decomposed in terms involving each amino acid. The residue-wise electrostatic energy was computed by switching on only the classical point charges of a particular residue, followed by an evaluation of the QM/MM electrostatic energy, without reoptimizing the wave function of the inhibitor. In order to evaluate the effects of the polarization, we used both the gas-phase (Ψ_0) and the polarized wave functions (Ψ) for the description of the inhibitor. The latter represents the wave function of the inhibitor polarized by the protein. In the present context, it should be noted that use of a nonpolarizable force field for the description of the protein could lead to an overestimation of the polarization effects. Nevertheless this is a common practice in present QM/MM studies.^{9,10}

RESULTS AND DISCUSSION

As previously underlined, the inhibitors notation in this work (L1 to L5) refer to their activity against the CK2 (see

Table 2. Average Bond Distances (\AA) and Their Standard Deviations between Each Inhibitor and Selected Amino Acids from the Active Site of CK2^a

	L1	L2A	L2B	L3	L4	L5
E114(O)-Br3	3.6 \pm 0.4 (3.4)	5.4 \pm 0.3 (3.1)	5.5 \pm 0.4 (5.4)	3.4 \pm 0.2 (5.4)	6.1 \pm 0.4 (6.6)	3.4 \pm 0.2
V116(O)-Br2	3.4 \pm 0.3 (3.2)	4.4 \pm 0.3 (3.3)	5.8 \pm 0.5 (5.3)	3.4 \pm 0.2 (5.3)	7.6 \pm 0.5 (7.0)	3.4 \pm 0.2
K68(NZ)-C1 or N2	6.8 \pm 0.5 (6.4)	4.2 \pm 0.2 (5.3)	9.5 \pm 0.4 (9.1)	4.6 \pm 0.3 (9.1)	3.2 \pm 0.2 (3.3)	5.0 \pm 0.3

^a Values in parentheses represent crystallographic data.

Table 1). In this section we start by presenting the structural features of all the inhibitors studied and their evolution during the QM/MM MD simulations. This is followed by an QM/MM-PB/SA analysis of the interaction energy between the protein and the inhibitors. Both geometrical and energy terms are averaged over 51 equispaced snapshots taken from the last 0.5 ns of the simulations if not specified otherwise.

The average distances with residues from the hinge region (E114(O)-Br3 and V116(O)-Br2) and the distance with polar residue K68 (K68(NZ)-C1 or N2) are given in Table 2. These values allowed us to follow the evolution of the inhibitors during the MD simulations.

Inhibitor L4. TBB (4,5,6,7-tetrabromobenzotriazole), denoted as L4 in this work, is one of the most widely used inhibitors of CK2. The analysis of the X-ray structure of CK2 complexed with different inhibitors leads Battistutta et al.²⁹ to notice a shift in the position of the inhibitor in the active site when compared with the tetrabromobenzimidazole derivatives K25 and K37, denoted in this study as L1 and L2, respectively. Due to this shift, no halogen bonds are established with the carbonyl backbone of residues E114 and V116 in the hinge region. The authors hypothesize that this different orientation is due to the distinct chemical properties of the five-membered ring, which would make L4 an anion at neutral pH. To test this assumption, we have performed two distinct simulations with the neutral and the anionic form of L4. The final structure for the two simulations together with the X-ray structure are shown in Figure 1. The evolution of the anionic and neutral form during the MD is indeed different. In the case of the neutral form, the triazole ring establishes two hydrogen bonds with the water molecules close to the active site. This leads to an in-plane clockwise rotation of the inhibitor relative to its initial position. Additionally, the initial halogen bonds of the inhibitor with residues E114 and V116 are shifted from Br3 and Br2 to Br2 and Br1.

On the other hand, for the anionic form of L4, we observed three hydrogen bonds between the five-membered ring and water molecules. One of these interactions is established with the water molecule that lies in-plane with the inhibitor and mediates the electrostatic interaction with the positively charged K68. This observation coupled with the fact that the anionic form of L4 has a C_{2v} symmetry explains its orientation for the first 0.9 ns of MD simulation. For this simulation interval the average distances with the residues from the hinge region are $3.7 \pm 0.4 \text{ \AA}$ for E114(O)-Br3 and $4.1 \pm 0.7 \text{ \AA}$ for V116(O)-Br2. For the last 0.5 ns of the MD simulation, we observed a different orientation in which the anionic form of L4 is shifted away from the hinge region toward the positively charged K68. The distance from the

hinge region residues increases, while the distance with K68 decreases (Figure 1d). This suggests that the electrostatic interaction is able to orient the inhibitor in the active site. The average distances for the production run are in good agreement with those measured from X-ray structure (Table 2).

It is worth mentioning the presence of two water molecules W1 and W2 in the active site of the anionic form. These water molecules occupy positions similar to the water molecules in the X-ray structure. No resident water molecules were observed in the case of protonated form. These observations suggest that the anionic form is most likely to be present at the neutral pH and that a relative long equilibration time, more than 1 ns, is required for these particular systems.

Inhibitors L3 and L5. These inhibitors have a fifth bromine atom which is bound to the C1 atom of imidazole ring. They differentiate by the fact that the hydrogen atom bound to N1 in L3 is replaced by an acetamido group in the case of L5. This acetamido group makes more interactions with the water molecules around the active site, shifting the position of the inhibitor during the course of the MD simulation, allowing water molecules to enter in the region between the inhibitor and the protein. In the case of L3 these interactions are reduced, and the occasional shift toward the exterior is not observed. For this inhibitor only one water molecule mediates the interaction with the protein. In the first 0.6 ns of the simulation, this water molecule flips between the positions W1 and W2. After this equilibration period the water molecule settles in the W2 position.

The final orientations of the two inhibitors are similar. This is reflected by the fact that the average distance with the residues from the hinge region are close (Table 2). Also it should be noted that no direct interaction is established with residue K68 as in the case of the anionic form of L4. For L3 and L5 this interaction is mediated by the water molecule W2, leading to an increase in the distance K68(NZ)-C1.

Inhibitors L1 and L2. These inhibitors have the highest inhibition constants in the series under study with L1 being the most potent one.²⁵ The position of L1 does not change dramatically during the course of the MD simulation, and the average distances for the whole 1.5 ns MD simulation are in good agreement with those from Table 2, $3.7 \pm 0.4 \text{ \AA}$ for E114(O)-Br3 distance, $3.5 \pm 0.3 \text{ \AA}$ for V116(O)-Br2 distance, and 6.7 ± 0.4 for the K68(NZ)-C1 distance. This can be explained by the fact that the starting structure for this simulation was the X-ray structure of CK2 complexed with this inhibitor. Secondly, we have seen that in the case of anionic or polar inhibitors, the orientation of the inhibitor in the active site is strongly influenced by the electrostatic

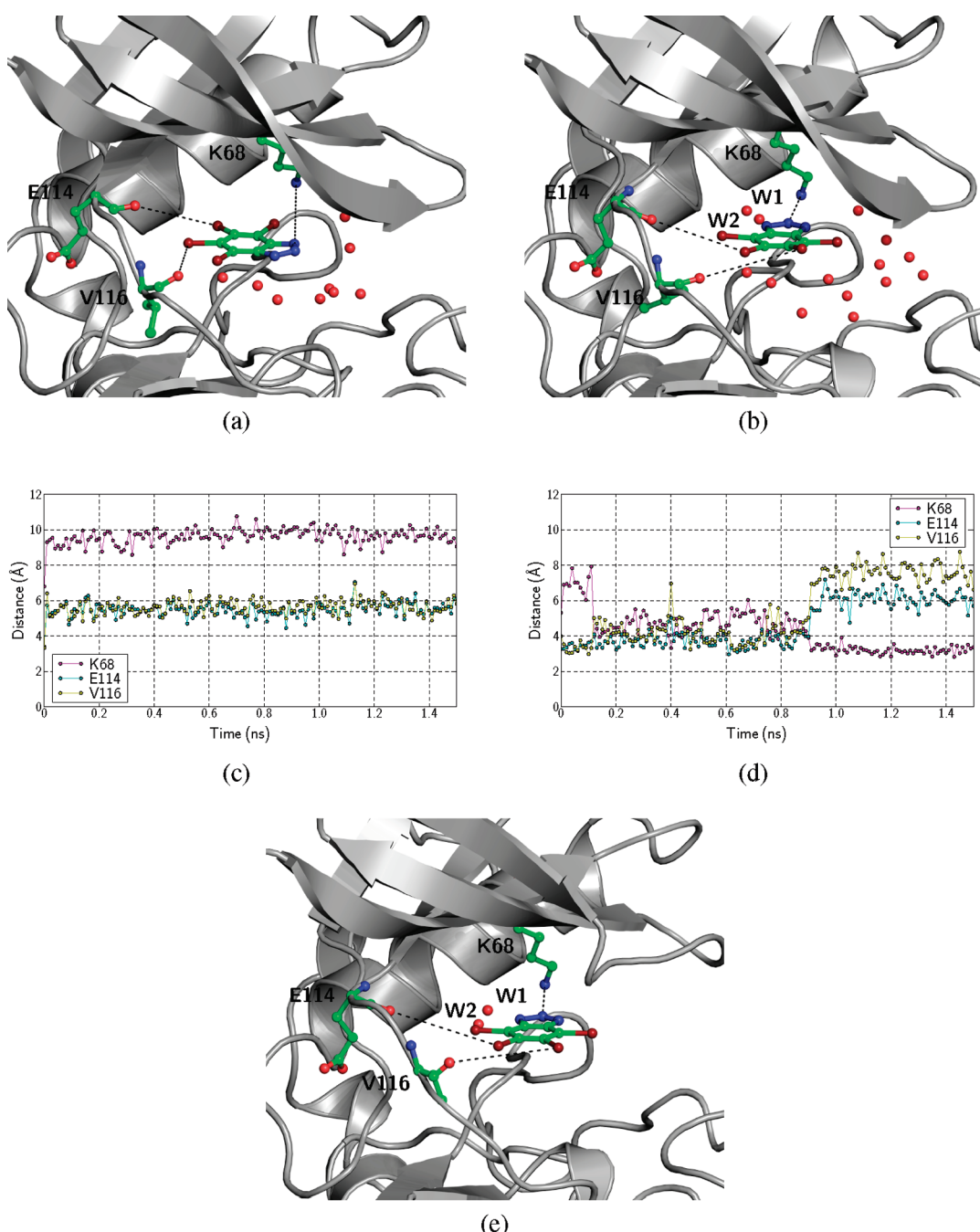


Figure 1. Final snapshot from the MD trajectory of CK2 complexed with L4 in its neutral form (a), anionic form (b), and crystal structure of the complex (e). The inhibitor, residues K68, E114, and V116, and all water molecules within 5 Å of the inhibitor are represented in a ball-and-stick model. The protein is represented with gray cartoons. Hydrogens are removed for clarity. Measured distances are depicted as black dashed lines. Evolution of the selected distances between the neutral form and CK2 and the anionic form and CK2 are depicted in parts (c) and (d), respectively.

interaction with the positively charged K68 (in the case of L4 anion) or by the hydrogen bonds formed with water molecules close to the active site (in the case of L4 neutral). For L1 the two CH_3 groups on the nitrogen atom hinder these interactions, and even the presence of a hydrogen bond ($\text{N}1-\text{H} \cdots \text{OH}_2$) cannot “overcome” the halogen bond interaction of the inhibitor with the residues from the hinge region.

In the case of L2, two distinct simulations were run (L2A and L2B), while changing only the random velocities generated at the beginning of the simulation. This was motivated by the fact that the crystal structure of CK2

complexed with L2 showed two possible orientations for this inhibitor in the active site of CK2.

In simulation L2A, even though at the beginning the CH_3 group on the sulfur atom was orientated toward residue K68, we noticed a flip after 0.2 ns (Figure 2c). This leads to a strong electrostatic interaction with residue K68 which reduces the distance K68(NZ)-C1 by more than 3 Å, when compared to the initial value. In the crystal structure this interaction is mediated by a water molecule, which leads to a placement of the inhibitor closer to the hinge region (Table 2).

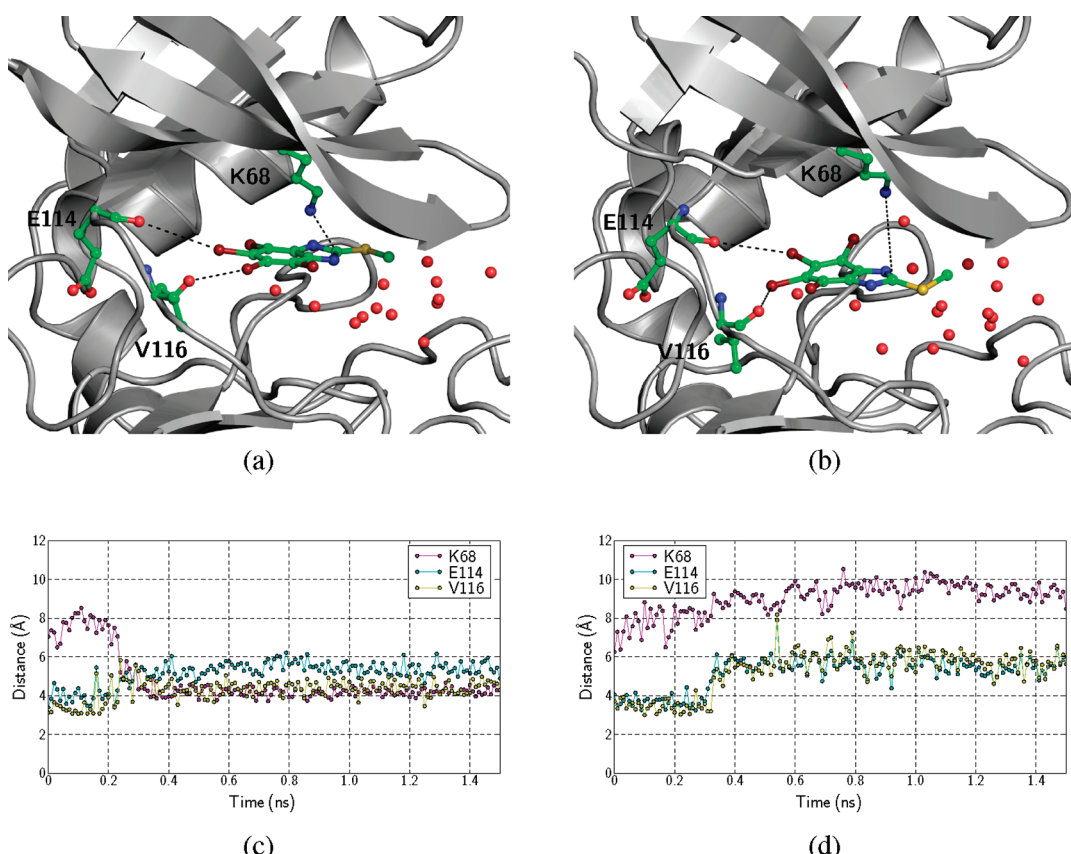


Figure 2. Final snapshot from the MD trajectory of CK2 complexed with L2 in simulation L2A (a) and simulation L2B (b). Representation is made as in Figure 1. Evolution of the selected distances between the inhibitor and CK2 in simulation L2A and simulation L2B are depicted in parts (c) and (d), respectively.

Table 3. Binding Energies and Standard Deviations of Averages Computed with the QM/MM-PB/SA Method^a

	L1	L2A	L2B	L3	L4	L5
ΔE_{elec}	2.8 ± 1.4	-4.5 ± 2.3	-6.8 ± 4.0	-4.0 ± 1.6	-104.2 ± 7.3	-13.0 ± 4.4
ΔE_{vdw}	-40.0 ± 1.7	-40.7 ± 1.9	-39.5 ± 1.6	-38.4 ± 1.5	-31.5 ± 1.5	-44.7 ± 1.5
ΔG_{PB}	5.0 ± 3.1	13.8 ± 3.2	14.9 ± 4.5	16.2 ± 1.7	108.9 ± 5.6	31.4 ± 4.8
ΔG_{SA}	-2.7 ± 0.1	-2.3 ± 0.1	-2.4 ± 0.1	-2.2 ± 0.1	-1.9 ± 0.1	-2.6 ± 0.1
ΔG_{polar}^b	7.9 ± 3.1	9.2 ± 3.1	8.1 ± 2.6	12.2 ± 2.2	4.7 ± 3.1	18.4 ± 3.0
$\Delta G_{nonpolar}^c$	-42.7 ± 1.7	-43.0 ± 1.9	-41.9 ± 1.6	-40.6 ± 1.5	-33.4 ± 1.5	-47.3 ± 1.5
$\Delta\Delta E_{QM/MM}^d$	0.0	-8.0	-9.1	-5.3	-98.5	-20.5
$\Delta\Delta G_{cal}^e$	0.0	1.1	1.0	6.5	6.1	6.0
$\Delta\Delta G_{exp}$	0.0	0.3	0.3	1.1	1.4	2.3

^a All energies are in kcal/mol. ^b $\Delta G_{polar} = \Delta E_{elec} + \Delta G_{PB}$. ^c $\Delta G_{nonpolar} = \Delta E_{vdw} + \Delta G_{SA}$. ^d $\Delta\Delta E_{QM/MM}$ refers to the relative QM/MM interaction energy; for each inhibitor $\Delta E_{QM/MM} = \Delta E_{elec} + \Delta E_{vdw}$. ^e $\Delta\Delta G_{cal}$ refers to the relative binding energy calculated with QM/MM-PB/SA method; for each inhibitor $\Delta G_{cal} = \Delta E_{elec} + \Delta E_{vdw} + \Delta G_{PB} + \Delta G_{SA}$.

For simulation L2B, the flip of the CH_3 group is not observed. As a result the inhibitor executes a clockwise rotation similar to that of the neutral form of L4 (Figure 2b) and exposes the imidazole ring to the solvent.

For both simulations, L2A and L2B, we find a good agreement between the averaged distances of the 0.5 ns production run and the X-ray values (Table 2).

Interaction Energies. The present QM/MM-PB/SA study allows us to analyze the individual energy components contributing to the total binding energy. Calculated values together with experimentally measured relative difference of free energy of binding are presented in Table 3.

In a previous study of CDK2 inhibitors, Tuñón et al. obtained a high coefficient of determination ($R^2 = 0.92$), when they expressed the activity as a function of QM/MM interaction energy.¹⁸ Based on their results, they concluded

that for inhibitors belonging to the same family the QM/MM interaction energy can be used as a predictor of biological activity.

We performed the same linear regression analysis, using the experimental binding energy ($\Delta\Delta G_{exp}$) and QM/MM interaction energy ($\Delta\Delta E_{QM/MM}$) as the input data set (for L2 only the calculated value from the B simulation was used to perform this analysis). In our case we obtain a value of 0.14 for R^2 . The poor correlation can be explained by taking a closer look at the individual electrostatic and van der Waals energies that are summed up to give $\Delta E_{QM/MM}$. Especially the calculated values for ΔE_{elec} show a large variation within this set of inhibitors. For example the presence of the acetamido group on L5 makes the electrostatic interaction approximately 9 kcal/mol larger when compared to L3. The van der Waals interaction energy also favors L5 by ap-

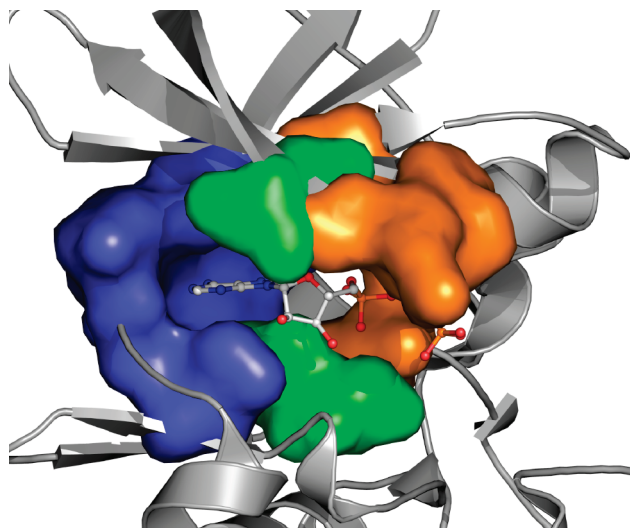


Figure 3. The X-ray structure of CK2 with AMPPNP (PDB code: 1DAW). The ANP is represented in a ball-and-stick model, while the CK2 protein is represented with gray cartoons. The adenine pocket (blue) comprise the residues I66, V95, F113, E114, Y115, V116, and M163. The ribose region (green) comprise the residues V45, V53, N161, and I174. The triphosphate binding region (orange) comprise the residues G46, R47, G48, S51, K68, and D175.

proximately 6 kcal/mol. On the contrary, experimental data disfavor L5 by -1.3 kcal/mol. The most striking finding of Table 3 is the value obtained for electrostatic interaction energy in the case of L4, which is 1 order of magnitude larger when compared with the other inhibitors. Due to the different polarities of these inhibitors, especially L4 and L5, it is very difficult to obtain a good correlation between experimental data and calculated $\Delta\Delta E_{QMM/MM}$ without taking into account the effects of both ligand and protein desolvation.

Within the traditional MM-PB/SA framework, it has been demonstrated that the solvation energy is a key element in correctly ranking inhibitors belonging to the same family. As can be seen in Table 3, the favorable electrostatic protein–inhibitor interaction energy is canceled by an unfavorable polar desolvation contribution (ΔG_{PB}), which has the largest value for L4 and L5. Because the absolute value of ΔE_{elec} is smaller, net positive polar components (ΔG_{pol}) are obtained for all inhibitors. Similarly, the nonpolar component of the protein–inhibitor binding free energy ($\Delta G_{nonpolar}$) can be regarded as the sum of the van der Waals energy term (ΔE_{vdW}) and the nonpolar term in the solvation energy (ΔG_{SA}). This quantity is a large negative number for all the inhibitors studied. As a result we can conclude that the latter is the driving force for the binding of these CK2 inhibitors. With the inclusion of solvation energy, the coefficient of determination resulting from the linear regression analysis is improved from $R^2 = 0.14$ to $R^2 = 0.69$. This clearly indicates the importance of solvation effects.

Contribution of Individual Amino Acids. The ATP-binding site of CK2 can be divided in three separate regions: the adenine pocket, the ribose region, and the triphosphate region (Figure 3). As can be seen from Table 4 the values resulted from the per-residue van der Waals interaction energy decomposition are influenced by the position of the inhibitor in the active site. L2A and L4 have the largest van der Waals interaction energy with residues from the triphosphate site. If we consider only the van der Waals

interaction energy coming from residues located in the adenine pocket, the situation is inversed. For the interaction with residues from the ribose region we find similar values for all inhibitors.

The high specificity of this family of inhibitors toward CK2 was attributed to the particularity of its ATP-binding site. Three of the residues found in the active site of CK2 (I66, M163, and I174) are specific to this protein and are replaced by less bulkier residues in other kinase. The importance of I66 and I174 was assessed by mutational studies in which they were individually or collectively mutated to one or more alanines.⁴² Interestingly, we find that these residues have the largest contribution to the final van der Waals interaction energy. Additionally residues V45, V53, V95, F113, and D175 were found to stabilize all the inhibitors but to a lesser extent. These results confirm the recent study of Nie et al.⁴³ With the addition of a nitrile group on a pyrazolo[1,5-a][1,3,5]triazine skeleton which interacts with the V95 and F113 hydrophobic residues, an ~ 10 -fold increase of the potency was observed.

While comparing different X-ray crystal structure of CK2 complexed with different inhibitors, Battistutta et al.²⁹ noticed a tendency of clustering around a unique zone of the ATP-binding pocket located near K68, for inhibitors that bear a negatively charged moiety. We have seen previously that this interaction can play an important role in orienting the inhibitors in the active site of the CK2. As can be seen from Table 5, K68 has a large contribution to the total electrostatic interaction energy. This interaction is more stabilizing in the case of L2A and L4. It should be noted that this favorable contribution is partially canceled by two unfavorable contributions coming from residues D81 and E175. The values from Table 5 also demonstrate the importance of polarization. For example in the case of electrostatic interaction between L2A and K68 the inhibitor is stabilized by more than 6 kcal/mol when the polarized wave function is used. Nie et al.⁴³ found that inhibitors that take advantage of these electrostatic interactions have an ~ 20 -fold increase in their inhibition power.

We note that the strongest inhibitor L1 fits perfectly in the adenine pocket of the protein, thus maximizing the van der Waals interaction, but has a weak electrostatic interaction with the charged residues clustered around K68. On the other hand, L2A has a strong electrostatic interaction with these residues. Due to this electrostatic interaction, the inhibitor shifts away from the hinge region, reducing the van der Waals interaction energy. Based on these observations we can state that the addition of sufficiently large polar group on the tetrabromobenzimidazole skeleton could increase the electrostatic interaction with the triphosphate binding region, while keeping the inhibitor close to the hinge region and thus maximizing the van der Waals interaction with the adenine pocket.

CONCLUSIONS

We have performed QM/MM molecular dynamics simulation to study the binding of a set of tetrabromobenzimidazole inhibitors to the CK2 protein. The QM representation of the ligand has a major advantage over a classical force field based methods in that it does not require derivation of empirical parameters for each ligand studied. Additionally

Table 4. Individual Amino Acid Residues Contribution to the van der Waals Interaction Energy

	residue	L1	L2A	L2B	L3	L4	L5
adenine pocket	I66	-4.1	-2.7	-4.1	-4.3	-2.4	-4.2
	V95	-1.3	-1.2	-1.5	-1.4	-0.8	-1.3
	F113	-2.8	-2.8	-2.8	-2.5	-1.9	-2.4
	E114	-1.0	-0.3	-1.1	-1.1	-0.3	-1.2
	Y115	-0.9	-0.2	-1.1	-1.3	-0.2	-1.2
	V116	-1.8	-2.3	-2.3	-2.6	-0.7	-2.5
	M163	-3.9	-2.3	-3.9	-3.6	-2.4	-4.4
	total	-15.8	-11.8	-16.7	-16.7	-8.7	-17.2
	V45	-1.5	-1.8	-3.0	-1.6	-1.7	-2.9
	V53	-3.1	-3.6	-3.1	-2.8	-3.7	-3.3
ribose region	N161	-0.7	-0.6	-0.4	-0.4	-0.5	-0.8
	I174	-4.9	-5.0	-4.6	-4.4	-4.3	-5.8
	total	-10.1	-10.9	-11.1	-9.2	-10.2	-12.8
	G46	-0.7	-1.2	-1.0	-0.6	-1.4	-1.3
	R47	-1.0	-1.3	-0.7	-0.4	-1.3	-0.7
triphosphate region	G48	-0.7	-0.7	-0.1	-0.2	-0.3	-0.1
	S51	-0.6	-1.1	-0.2	-0.6	-0.6	-0.4
	K68	-1.7	-3.5	-1.4	-2.2	-2.0	-1.8
	D175	-2.3	-3.4	-1.7	-2.1	-2.5	-1.9
	total	-6.9	-11.1	-5.2	-6.1	-8.0	-6.3

^a All energies are in kcal/mol.

Table 5. Individual Amino Acid Contribution to the Electrostatic Interaction Energy Calculated Using the Gas-Phase (Ψ_0) and the Polarized (Ψ) Semiempirical Wavefunction for the Description of the Inhibitor^a

residue	L1		L2A		L2B		L3		L4		L5	
	Ψ_0	Ψ										
K68	0.0	-2.7	-15.0	-21.2	-2.1	-4.3	-5.2	-9.8	-76.1	-84.1	-4.4	-9.1
D81	0.5	1.6	4.6	7.1	1.5	2.4	1.8	3.7	43.4	46.2	1.6	3.6
E175	-3.0	0.0	3.8	8.2	1.3	3.7	-1.6	2.7	55.4	60.5	-0.1	4.0

^a All energies are in kcal/mol.

the polarization of the wave function by the environment is also taken into account.

The resulting molecular dynamics trajectories were analyzed combining QM/MM with the Poisson–Boltzmann/surface area (PB/SA) model for the representation of solvation effects. For the studied inhibitors, the QM/MM-PB/SA analysis indicates that the van der Waals interactions have the largest contribution to the binding, while the electrostatic interactions play an important role in the orientation of each individual ligand inside the binding pocket. These results not only are in agreement with experimental observations of Battistutta et al.²⁸ but also provide a quantitative picture for the interactions responsible for the protein–ligand binding. The inclusion of solvation effects proved to be essential for the proper damping of electrostatic interactions. Their importance is clearly demonstrated by the coefficient of determination resulted from the linear regression analysis between the experimental binding energy and the calculated one. The value of R^2 is greatly improved from 0.14, for the case when only the QM/MM interaction energy is used, to 0.69 when solvation effects are also taken into account.

Finally the van der Waals and electrostatic interaction energies were decomposed in terms pertaining to each amino acid. Based on the information provided by this analysis we propose a way for improving the current inhibitors, by taking advantage of the electrostatic interaction with the residues located around K68. We suggest that the addition of a sufficiently large polar group on the tetrabromobenzimidazole skeleton could increase this electrostatic interaction without

losing the favorable van der Waals interactions with the bulky residues I66, M163, and I174 specific to the CK2.

The results obtained for these systems suggest that the QM/MM-PB/SA method can be successfully applied to quantify the protein–ligand interaction energies and might be employed in the design of new inhibitors.

ACKNOWLEDGMENT

The authors thank Aline Thomas and Martin Field for their advice on using the fDynamo library and the CECIC center for providing computer facilities.

REFERENCES AND NOTES

- Jorgensen, W. L. The Many Roles of Computation in Drug Discovery. *Science* **2004**, *303*, 1813–1818.
- Gohlke, H.; Klebe, G. Statistical potentials and scoring functions applied to protein-ligand binding. *Curr. Opin. Struct. Biol.* **2001**, *11*, 231–235.
- Kollman, P. Free energy calculations: Applications to chemical and biochemical phenomena. *Chem. Rev.* **1993**, *93*, 2395–2417.
- Beveridge, D. L.; DiCapua, F. M. Free energy via molecular simulation: applications to chemical and biomolecular systems. *Annu. Rev. Biophys. Biomol. Chem.* **1989**, *18*, 431–492.
- Åqvist, J.; Medina, C.; Samuelsson, J.-E. A new method for predicting binding affinity in computer-aided drug design. *Protein Eng.* **1994**, *7*, 385–391.
- Hansson, T.; Marelius, J.; Åqvist, J. Ligand binding affinity prediction by linear interaction energy methods. *J. Comput.-Aided Mol. Des.* **1998**, *12*, 27–35.
- Kollman, P. A.; Massova, I.; Reyes, C.; Kuhn, B.; Huo, S.; Chong, L.; Lee, M.; Lee, T.; Duan, Y.; Wang, W.; Donini, O.; Cieplak, P.; Srinivasan, J.; Case, D. A.; Cheatham, T. E. Calculating structures and free energies of complex molecules: combining molecular

- mechanics and continuum models. *Acc. Chem. Res.* **2000**, *33*, 889–897.
- (8) Garcia-Viloca, M.; Truhlar, D. G.; Gao, J. Importance of Substrate and Cofactor Polarization in the Active Site of Dihydrofolate Reductase. *J. Mol. Biol.* **2003**, *327*, 549–560.
- (9) Hensen, C.; Hermann, J. C.; Nam, K.; Ma, S.; Gao, J.; Höltje, H.-D. A combined QM/MM approach to protein-ligand interactions: polarization effects of the HIV-1 protease on selected high affinity inhibitors. *J. Med. Chem.* **2004**, *47*, 6673–6680.
- (10) Alves, C. N.; Martí, S.; Castillo, R.; Andrés, J.; Moliner, V.; Tuñón, I.; Silla, E. A Quantum Mechanic/Molecular Mechanic Study of the Wild-Type and N155S Mutant HIV-1 Integrase Complexed with Diketo Acid. *Biophys. J.* **2008**, *94*, 2443–2451.
- (11) Warshel, A.; Levitt, M. Theoretical studies of enzymic reactions: dielectric, electrostatic and steric stabilization of the carbonium ion in the reaction of lysozyme. *J. Mol. Biol.* **1976**, *103*, 227–249.
- (12) Field, M. J.; Bash, P. A.; Karplus, M. A combined quantum mechanical and molecular mechanical potential for molecular dynamics simulations. *J. Comput. Chem.* **1990**, *11*, 700–733.
- (13) Field, M. J. Simulating enzyme reactions: Challenges and perspectives. *J. Comput. Chem.* **2002**, *23*, 48–58.
- (14) Gao, J.; Truhlar, D. G. Quantum mechanical methods for enzyme kinetics. *Annu. Rev. Phys. Chem.* **2002**, *53*, 467–505.
- (15) Senn, H. M.; Thiel, W. QM/MM studies of enzymes. *Curr. Opin. Chem. Biol.* **2007**, *11*, 182–187.
- (16) Raha, K.; Peters, M. B.; Wang, B.; Yu, N.; Wollacott, A. M.; Westerhoff, L. M.; Merz, K. M. The Role of Quantum Mechanics in Structure-Based Drug Design. *Drug Discovery Today* **2007**, *12*, 725–731.
- (17) Khandelwal, A.; Lukacova, V.; Comez, D.; Kroll, D. M.; Raha, S.; Balaz, S. A Combination of Docking, QM/MM Methods, and MD Simulation for Binding Affinity Estimation of Metalloprotein Ligands. *J. Med. Chem.* **2005**, *48*, 5437–47.
- (18) Alzate-Morales, J. H.; Contreras, R.; Soriano, A.; Tuñón, I.; Silla, E. A Computational Study of the Protein-Ligand Interactions in CDK2 Inhibitors: Using Quantum Mechanics/Molecular Mechanics Interaction Energy as a Predictor of the Biological Activity. *Biophys. J.* **2007**, *92*, 430–439.
- (19) Gräter, F.; Schwarzl, S. M.; Dejaegere, A.; Fischer, S.; Smith, J. C. Protein/ligand binding free energies calculated with quantum mechanics/molecular mechanics. *J. Phys. Chem. B* **2005**, *109*, 10474–10483.
- (20) Kaukonen, M.; Söderhjelm, P.; Heimdal, J.; Ryde, U. QM/MM-PBSA Method To Estimate Free Energies for Reactions in Proteins. *J. Phys. Chem. B* **2008**, *112*, 12537–12548.
- (21) Manning, G.; Whyte, D. B.; Martinez, R.; Hunter, T.; Sudarsanam, S. The Protein Kinase Complement of the Human Genome. *Science* **2002**, *298*, 1912–1934.
- (22) Meggio, F.; Pinna, L. A. One-thousand-and-one substrates of protein kinase CK2. *FASEB J.* **2003**, *17*, 349–368.
- (23) Tawfic, S.; Yu, S.; Wang, H.; Faust, R.; Davis, A.; Ahmed, K. Protein kinase CK2 signal in neoplasia. *Histol. Histopathol.* **2001**, *16*, 573–582.
- (24) Ruzzene, M.; Penzo, D.; Pinna, L. A. Protein kinase CK2 inhibitor 4,5,6,7-tetrabromobenzotriazole (TBB) induces apoptosis and caspase-dependent degradation of haematopoietic lineage cell-specific protein 1 (HS1) in Jurkat cells. *Biochem. J.* **2002**, *364*, 41–47.
- (25) Pagano, M. A.; Andrzejewska, M.; Ruzzene, M.; Sarno, S.; Cesaro, L.; Bain, J.; Elliott, M.; Meggio, F.; Kazimierczuk, Z.; Pinna, L. A. Optimization of protein kinase CK2 inhibitors derived from 4,5,6,7-tetrabromobenzimidazole. *J. Med. Chem.* **2004**, *47*, 6239–6247.
- (26) Sarno, S.; de Moliner, E.; Ruzzene, M.; Pagano, M. A.; Battistutta, R.; Bain, J.; Fabbro, D.; Schoepfer, J.; Elliott, M.; Furet, P.; Meggio, F.; Zanotti, G.; Pinna, L. A. Biochemical and three-dimensional-structural study of the specific inhibition of protein kinase CK2 by [5-oxo-5,6-dihydroindolo-(1,2-a)quinazolin-7-yl]acetic acid (IQA). *Biochem. J.* **2003**, *374*, 639–646.
- (27) Battistutta, R.; Moliner, E. D.; Sarno, S.; Zanotti, G.; Pinna, L. A. Structural features underlying selective inhibition of protein kinase CK2 by ATP site-directed tetrabromo-2-benzotriazole. *Protein Sci.* **2001**, *10*, 2200–2206.
- (28) Battistutta, R.; Mazzorana, M.; Sarno, S.; Kazimierczuk, Z.; Zanotti, G.; Pinna, L. A. Inspecting the Structure-Activity Relationship of Protein Kinase CK2 Inhibitors Derived from Tetrabromo-Benzimidazole. *Chem. Biol.* **2005**, *12*, 1211–1219.
- (29) Battistutta, R.; Mazzorana, M.; Cendron, L.; Bortolato, A.; Sarno, S.; Kazimierczuk, Z.; Zanotti, G.; Moro, S.; Pinna, L. A. The ATP-Binding Site of Protein Kinase CK2 Holds a Positive Electrostatic Area and Conserved Water Molecules. *ChemBioChem* **2007**, *8*, 1804–1809.
- (30) Sarno, S.; Reddy, H.; Meggio, F.; Ruzzene, M.; Davies, S. P.; Donella-Deana, A.; Shugar, D.; Pinna, L. A. Selectivity of 4,5,6,7-tetrabromobenzotriazole, an ATP site-directed inhibitor of protein kinase CK2 ('casein kinase-2'). *FEBS Lett.* **2001**, *496*, 44–48.
- (31) Schaftenaar, G.; Noordik, J. Molden: a pre- and post-processing program for molecular and electronic structures. *J. Comput.-Aided Mol. Des.* **2000**, *14*, 123–134.
- (32) Dolinsky, T. J.; Nielsen, J. E.; McCammon, J. A.; Baker, N. A. PDB2PQR: an automated pipeline for the setup of Poisson-Boltzmann electrostatics calculations. *Nucleic Acids Res.* **2004**, *32*, 665–667.
- (33) Li, H.; Robertson, A. D.; Jensen, J. H. Very fast empirical prediction and rationalization of protein pKa values. *Proteins* **2005**, *61*, 704–721.
- (34) Field, M. J.; Albe, M.; Bret, C.; Martin, F. P.-D.; Thomas, A. The dynamo library for molecular simulations using hybrid quantum mechanical and molecular mechanical potentials. *J. Comput. Chem.* **2000**, *21*, 1088–1100.
- (35) Dewar, M. J. S.; Zoebisch, E. G.; Healy, E. F.; Stewart, J. J. P. Development and use of quantum mechanical molecular models. 76. AM1: a new general purpose quantum mechanical molecular model. *J. Am. Chem. Soc.* **1993**, *115*, 5348–5348.
- (36) Jorgensen, W.; Maxwell, D.; Tirado-Rives, J. Development and Testing of the OPLS All-Atom Force Field on Conformational Energetics and Properties of Organic Liquids. *J. Am. Chem. Soc.* **1996**, *118*, 11225–11236.
- (37) Jorgensen, W. L.; Chandrasekhar, J.; Madura, J. D.; Impey, R. W.; Klein, M. L. Comparison of simple potential functions for simulating liquid water. *J. Chem. Phys.* **1983**, *79*, 926–935.
- (38) Srinivasan, J.; Cheatham, T.; Cieplak, P.; Kollman, P.; Case, D. Continuum Solvent Studies of the Stability of DNA, RNA, and Phosphoramidate-DNA Helices. *J. Am. Chem. Soc.* **1998**, *120*, 9401–9409.
- (39) Gilson, M. K.; Honig, B. Calculation of the total electrostatic energy of a macromolecular system: Solvation energies, binding energies, and conformational analysis. *Proteins* **1988**, *4*, 7–18.
- (40) Frisch, M. J.; Trucks, G. W.; Schlegel, H. B.; Scuseria, G. E.; Robb, M. A.; Cheeseman, J. R.; Montgomery, J. A., Jr.; Vreven, T.; Kudin, K. N.; Burant, J. C.; Millam, J. M.; Iyengar, S. S.; Tomasi, J.; Barone, V.; Mennucci, B.; Cossi, M.; Scalmani, G.; Rega, N.; Petersson, G. A.; Nakatsuji, H.; Hada, M.; Ehara, M.; Toyota, K.; Fukuda, R.; Hasegawa, J.; Ishida, M.; Nakajima, T.; Honda, Y.; Kitao, O.; Nakai, H.; Klene, M.; Li, X.; Knox, J. E.; Hratchian, H. P.; Cross, J. B.; Bakken, V.; Adamo, C.; Jaramillo, J.; Gomperts, R.; Stratmann, R. E.; Yazyev, O.; Austin, A. J.; Cammi, R.; Pomelli, C.; Ochterski, J. W.; Ayala, P. Y.; Morokuma, K.; Voth, G. A.; Salvador, P.; Dannenberg, J. J.; Zakrzewski, V. G.; Dapprich, S.; Daniels, A. D.; Strain, M. C.; Farkas, O.; Malick, D. K.; Rabuck, A. D.; Raghavachari, K.; Foresman, J. B.; Ortiz, J. V.; Cui, Q.; Baboul, A. G.; Clifford, S.; Cioslowski, J.; Stefanov, B. B.; Liu, G.; Liashenko, A.; Piskorz, P.; Komaromi, I.; Martin, R. L.; Fox, D. J.; Keith, T.; Al-Laham, M. A.; Peng, C. Y.; Nanayakkara, A.; Challacombe, M.; Gill, P. M. W.; Johnson, B.; Chen, W.; Wong, M. W.; Gonzalez, C.; Pople, J. A. *Gaussian 03, Revision C.02*; Gaussian, Inc.: Wallingford, CT, 2004.
- (41) Sitkoff, D.; Sharp, K. A.; Honig, B. Accurate Calculation of Hydration Free Energies Using Macroscopic Solvent Models. *J. Phys. Chem.* **1994**, *98*, 1978–1988.
- (42) Meggio, F.; Pagano, M.; Moro, S.; Zagotto, G.; Ruzzene, M.; Sarno, S.; Cozza, G.; Bain, J.; Elliott, M.; Deana, A.; Brunati, A.; Pinna, L. Inhibition of Protein Kinase CK2 by Condensed Polyphenolic Derivatives. An In Vitro and in Vivo Study. *Biochemistry* **2004**, *43*, 12931–12936.
- (43) Nie, Z.; Perretta, C.; Erickson, P.; Margosiak, S.; Almassy, R.; Lu, J.; Averill, A.; Yager, K. M.; Chu, S. Structure-based design, synthesis, and study of pyrazolo[1,5-a][1,3,5]triazine derivatives as potent inhibitors of protein kinase CK2. *Bioorg. Med. Chem. Lett.* **2007**, *17*, 4191–4195.